GPS Solut (2014) 18:323–333
DOI 10.1007/s10291-014-0371-y

REVIEW ARTICLE

Impact of GLONASS pseudorange inter-channel biases on satellite clock corrections

Weiwei Song · Wenting Yi · Yidong Lou · Chuang Shi · Yibin Yao · Yanyan Liu · Yong Mao · Yu Xiang

Received: 27 November 2013 / Accepted: 22 February 2014 / Published online: 21 March 2014

Abstract GLONASS carrier phase and pseudorange observations suffer from inter-channel biases (ICBs) because of frequency division multiple access (FDMA). Therefore, we analyze the effect of GLONASS pseudorange inter-channel biases on the GLONASS clock corrections. Different Analysis Centers (AC) eliminate the impact of GLONASS pseudorange ICBs in different ways. This leads to significant differences in the satellite and AC-specific offsets in the GLONASS clock corrections. Satellite and AC-specific offset differences are strongly correlated with frequency. Furthermore, the GLONASS pseudorange ICBs also leads to day-boundary jumps in the GLONASS clock corrections for the same analysis center between adjacent days. This in turn will influence the accuracy of the combined GPS/GLONASS precise point positioning (PPP) at the day-boundary. To solve these problems, a GNSS clock correction combination method based on the Kalman filter is proposed. During the combination, the AC-specific offsets and the satellite and AC-specific offsets can be estimated. The test results show the feasibility and effectiveness of the proposed clock combination method. The combined clock corrections can effectively weaken the influence of clock day-boundary jumps on combined GPS/GLONASS kinematic PPP. Furthermore, these combined clock corrections can improve the accuracy of the combined GPS/GLONASS static PPP single-day solutions when compared to the accuracy of each analysis center alone.

Keywords GLONASS · Clock corrections · Day-boundary jump · Inter-channel bias · Clock combination

W. Song · W. Yi (✉) · Y. Lou (✉) · C. Shi · Y. Liu · Y. Xiang
Research Center of GNSS, Wuhan University, 129 Luoyu Road, Wuhan 430079, China
e-mail: WtYi@whu.edu.cn

Y. Lou
e-mail: ydLou@whu.edu.cn

Y. Yao
School of Geodesy and Geomatics, Wuhan University, Wuhan 430079, China

Y. Mao
PetroChina West East Gas Pipeline Company, Shanghai, China

Introduction

The availability of precise satellite orbit and clock products has enabled the development of precise point positioning (PPP). This data processing technique can achieve positioning accuracy for static and mobile receivers at the millimeter to decimeter levels and has been widely applied in precise orbit determination, geodesy, aerial photogrammetry, sea level measurement, GPS meteorology and precise timing (Zumberge et al. 1997; Bisnath and Gao 2008; Kouba and Héroux 2001; Kouba 2003). Furthermore, with the revival of GLONASS and the increasing number of combined GPS/GLONASS receivers along with the availability of combined GPS/GLONASS orbit and satellite clock corrections, PPP can now be extended to include GLONASS measurements. The first tests on combined GPS/GLONASS PPP were presented by Cai and Gao (2007). However, they could not make a significant improvement in PPP since only two or three GLONASS satellites could be used. Hesselbarth and Wanninger (2008) tested GPS-only and combined GPS/GLONASS PPP using kinematic observations. Both studies demonstrated that adding GLONASS measurements to GPS can significantly

Table 1 Precise clock products for GPS/GLONASS PPP

ACs	Interval	Process strategy for GLONASS pseudorange inter-channel biases	Available time
IAC	30 s	Estimated with clock estimation	Since Jan 2005 or earlier
ESOC	5 min*	Estimated with clock estimation	Since Oct 19, 2008
GFZ	5 min**	Estimated with clock estimation	Since Apr 11, 2010
NRCan	30 s	Not estimated	Since Jun 3, 2012

The symbol * represents the ESOC provided the precise clock corrections in 30-s interval since January 24, 2010, while ** represents the GFZ provided the precise clock corrections in 30-s interval since June 2, 2013, but the last epoch is still 23:55:00

reduce the time for PPP convergence. Píriz et al. (2009) used 1-h static data from the International GNSS Service (IGS) to assess PPP. This research showed that GLONASS-only PPP solution in 1 h is not very reliable in some case, and a combined GPS/GLONASS PPP solution is more accurate and robust than the GPS-only solution.

The IGS is the main source of post-mission precise satellite orbit and clock products. To provide more reliable and stable clock correction solutions, IGS combines clock corrections from several participating Analysis Centers (AC) (Kouba 2003). It offers precise GPS satellite clock corrections, but does not provide GLONASS clock corrections. Until now, GLONASS satellite clock corrections were available only from the Information-Analytical Center (IAC), the European Space Operation Center (ESOC), the German Research Centre for Geosciences (GFZ) and Natural Resources Canada (NRCan), the product information is listed in Table 1.

At present, GLONASS uses frequency division multiplexing (FDMA-frequency division multiple access) to distinguish signals from individual satellites and only GLONASS FDMA signals will be able to provide continuous dual-frequency coverage for the next decade. However, with the FDMA approach, GLONASS carrier phase and pseudorange observations suffer from inter-channel biases. The carrier phase inter-channel biases between receivers from different manufacturers can reach up to 5 cm for adjacent frequencies and thus up to 73 cm for the complete L1 or L2 frequency bands (Wanninger 2012). Fortunately, carrier phase inter-channel biases seem stable over time and can be modeled as linear frequency functions. But pseudorange inter-channel biases seem to be unique to individual receivers and antennas. Moreover, they cannot be modeled with a simple modeling function (Reussner and Wanninger 2011, Chuang et al. 2013). Nevertheless, time reference synchronization is typically achieved by using estimated receiver and satellite clock corrections derived from the pseudorange observations, given the existence of ambiguities in carrier phase observations (Bock et al. 2009).

GLONASS pseudorange observations are affected by inter-channel biases (ICBs), so different pseudorange ICB processing strategies may lead the GLONASS clock reference to vary between different analysis centers. We analyze the effects of GLONASS pseudorange ICBs on GLONASS clock references and propose a combined GNSS clock method counterpoising the satellite and AC-specific offset and day-boundary jump impacts on GLONASS clock corrections. Section 2 analyzes the impacts of GLONASS pseudorange ICBs on the clock reference of GLONASS; Sect. 3 discusses the differences in the satellite and AC-specific offsets of the GLONASS clock between different analysis centers and the relationship of these differences with frequency; Sect. 4 analyzes day-boundary jumps of GLONASS clock corrections for each analysis center and their impact on the combined GPS/GLONASS PPP at the day-boundary; Sect. 5 presents some preliminary test results and discusses the feasibility and effectiveness of the proposed clock combination method.

GLONASS pseudorange ICBs impact on clock reference

Clock references are determined by pseudorange observations, and highly precise carrier phase observations determine only the accurate temporal change in clock corrections (Ge et al. 2012). Therefore, a linearized observation equation for the ionosphere-free pseudorange combination can be expressed as (somewhat simplified and without an error term):

$$P_c^i = \rho^i + c\mathrm{d}t_r - c\mathrm{d}t^i + m^i \mathrm{d}T + ICB^i \quad (1)$$

where i is the satellite PRN, P_c is the ionosphere-free pseudorange observation, ρ is the range from satellite to receiver, c is the speed of light in vacuum, $\mathrm{d}t_r$ and $\mathrm{d}t^i$ are receiver and satellite clock biases, m is the tropospheric mapping function, $\mathrm{d}T$ is the zenith troposphere delay, ICB is the inter-channel pseudorange bias.

In clock estimation, the station coordinates, satellite orbits and troposphere are assumed to be known. So:

$$V_{Pc}^i = c\mathrm{d}t_r - c\mathrm{d}t^i + ICB^i + l_{Pc}^i \quad (2)$$

where V_{Pc}^i and l_{Pc}^i are the post-fit and prefit residuals of the pseudorange observations. Since there are no pseudorange ICBs for GPS, Eq. (2) can be written as:

$$V_{Pc}^i = c\mathrm{d}t_r - c\mathrm{d}t^i + l_{Pc}^i \quad (3)$$

Equation (3) shows that the receiver and satellite clock biases are linear dependent and cannot be separated

from each other. However, there is no real clock reference. To obtain the satellite clock corrections, one or some stations equipped with atomic clocks are selected as the reference stations and their receiver clock biases are fixed as the clock references. Then the satellite clock biases are calculated, while the other receiver clock biases are related to the clock references (Zhang et al. 2010). Unfortunately, the GLONASS pseudorange observations are affected by pseudorange ICBs and the effects are difficult to completely eliminate (Reussner and Wanninger 2011, Chuang et al. 2013, Kozlov et al. 2000). Assuming that the uncalibrated ICBs are δICB^i, then (2) can be rewritten as:

$$V_{Pc}^i = c\mathrm{d}t_r - c\mathrm{d}t^i + \delta ICB^i + l_{Pc}^i \tag{4}$$

Not only are the satellite and receiver clock biases linear dependent as shown in (3), but also δICB^i has a linear dependency with the satellite and receiver clock biases. Moreover, the pseudorange ICBs vary for different satellites. The shared portion of all satellite δICB^i will be absorbed into the receiver clock biases, while the remaining portion of all satellite δICB^i will be absorbed into the satellite clock biases and affect the clock reference. Equation (4) can be rewritten as:

$$V_{Pc}^i = c\mathrm{d}\tilde{t}_r - c\mathrm{d}\tilde{t}^i + l_{Pc}^i \tag{5}$$

where $\mathrm{d}\tilde{t}_r$ and $\mathrm{d}\tilde{t}^i$ are receiver and satellite clock biases which contain the effects of the pseudorange ICB residuals.

The GLONASS clock references contain the residual pseudorange ICBs that cannot be eliminated, so the clock corrections for each analysis center can be expressed as follows

$$c_a^s = c^s + o_a + o_a^s \tag{6}$$

where c_a^s is clock correction for satellite s, c^s is the clock correction for satellite s estimated by carrier phase observations, o_a is the AC-specific clock offset (common for all satellites), o_a^s is the satellite and AC-specific clock offset (Mervart and Weber 2011).

Satellite and AC-specific offset analysis

The effects of pseudorange ICBs on the GLONASS clock reference may be different for different analysis centers since they select different reference stations as well as different pseudorange ICBs processing strategies. The difference in (6) between the analysis centers shows that:

$$\nabla c_{a,b}^s = \nabla c^s + \nabla o_{a,b} + \nabla o_{a,b}^s \tag{7}$$

where ∇ represents the single difference operator between analysis centers a and b. Assume that $\nabla c^s = 0$, since $\nabla o_{a,b}$ is common to all satellites, then:

$$\begin{aligned} \nabla o_{a,b} &= \frac{1}{n}\sum_{i=1}^{n} \nabla c_{a,b}^s \\ \nabla o_{a,b}^s &= \nabla c_{a,b}^s - \frac{1}{n}\sum_{i=1}^{n} \nabla c_{a,b}^s \end{aligned} \tag{8}$$

where n is the number of satellites.

Figure 1 shows a time series of GPS and GLONASS $\nabla o_{a,b}^s$ between the NRCan, ESOC and GFZ analysis centers and the IAC analysis center on day of year (DOY) 153 in 2013. In this figure, the GPS $\nabla o_{a,b}^s$ are all close to zero, but the GLONASS $\nabla o_{a,b}^s$ can reach several nanoseconds and vary for different satellites, which indicates the satellite and AC-specific offsets of GPS clock corrections are almost the same for all analysis centers while that of GLONASS vary for each analysis center. This is because different analysis centers possibly select different reference stations. However, since GPS is not affected by pseudorange ICBs, only different reference stations leads the AC-specific offsets to vary. But for GLONASS, the pseudorange ICBs can reach several meters which differ with reference stations (Reussner and Wanninger 2011; Chuang

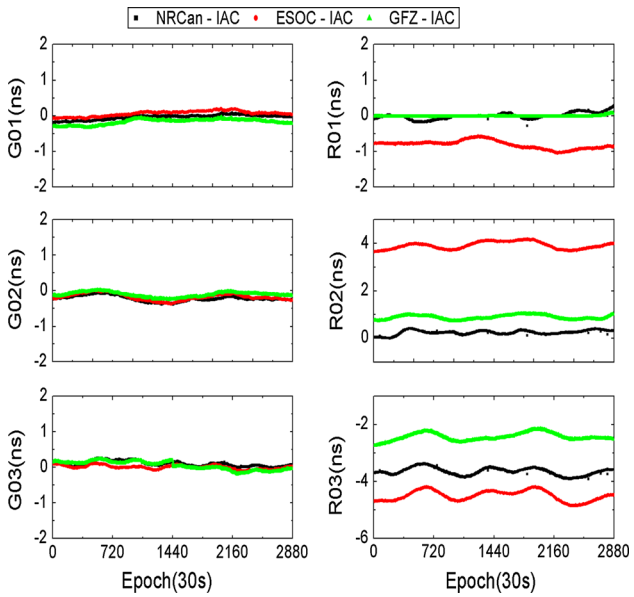

Fig. 1 Time series of $\nabla o_{a,b}^s$ between NRCan, ESOC and GFZ analysis centers and IAC analysis center on day of year (DOY) 153 in 2013. The *left panel* shows the time series for GPS satellites G01, G02 and G03, and the *right panel* displays the time series for GLONASS satellites R01, R02 and R03

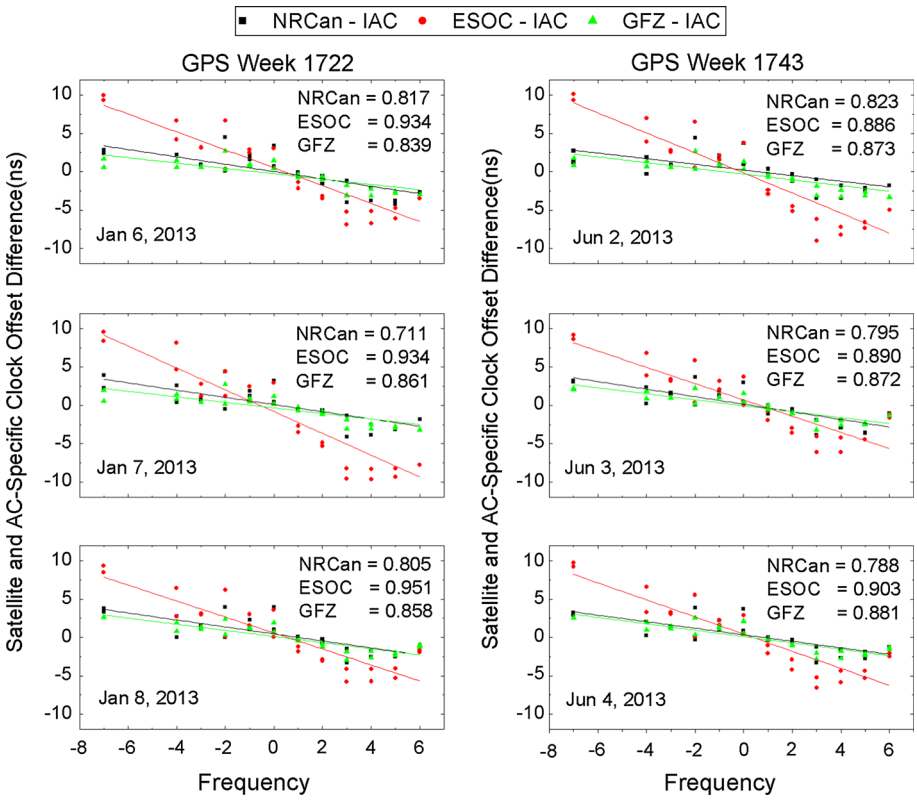

Fig. 2 GLONASS $\nabla o^s_{a,b}$ over three consecutive days for GPS week 1,722 and 1,743 for different analysis centers. In order to show the relationship between $\nabla o^s_{a,b}$ and frequency more clearly, the *fitted lines* and the correlation coefficients are also shown in this figure

et al. 2013). Meanwhile, different analysis centers process the pseudorange ICBs in different ways, so the impacts of the residual pseudorange ICBs on clock correction references vary, subsequently the satellite and AC-specific offsets vary for each analysis center.

Assume that o^s_a is constant within a 24-h period. Therefore, the average $\nabla o^s_{a,b}$ for each satellite can be computed. Figure 2 shows the relationship of GLONASS $\nabla o^s_{a,b}$ for different analysis centers and frequencies over three consecutive days for GPS week 1,722 and 1,743. In Fig. 2, the GLONASS$\nabla o^s_{a,b}$ for the two satellites sharing the same frequency are quite close. Furthermore, $\nabla o^s_{a,b}$ has a significant linear correlation with frequency, the average correlation coefficients between $\nabla o^s_{a,b}$ and the fitting straight line for NRCan, ESOC and GFZ analysis centers reach 0.790, 0.916 and 0.864, respectively. The frequency-dependent errors in pseudorange observations stem from ionospheric delay and ICBs. Since clock estimation usually uses ionosphere-free combination observations to eliminate the ionospheric delay effects (Ge et al. 2012; Bock et al. 2009; Kouba 2003), so $\nabla o^s_{a,b}$ is strongly correlated with frequency, confirming that the satellite and AC-specific offset is affected by pseudorange ICBs. However, the degree of correlation between $\nabla o^s_{a,b}$ and the frequency differs for different analysis centers. This is possibly due to the different pseudorange ICBs processing strategies. The

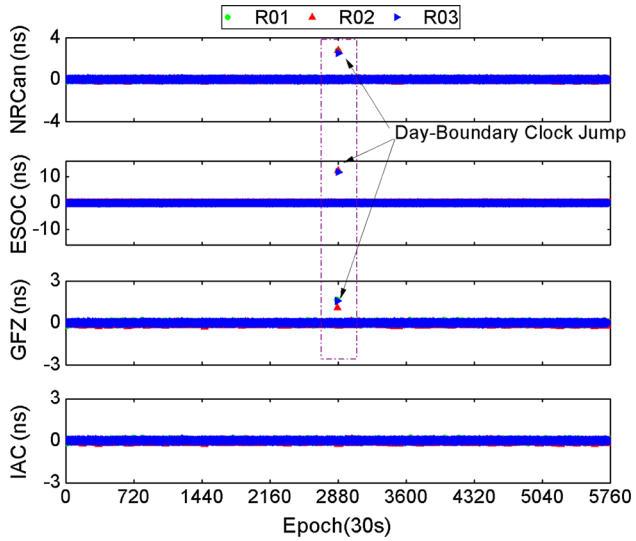

Fig. 3 Time series for clock differences between adjacent epochs of GLONASS R01, R02 and R03 for each analysis center on DOY 154 and 155 in 2013. The clock corrections for the GFZ analysis center were extrapolated to 23:59:30 since the last epoch of clock corrections for the GFZ analysis center is 23:55:00

ESOC, GFZ and IAC analysis centers add the additional pseudobias parameters during clock estimation but NRCan analysis center does not (ftp://igsws.unavco.org/pub/center/analysis/gfz.acn, esa.acn, emr.acn, iac.acn).

Day-boundary jumps analysis

Figure 3 shows the time series of clock correction differences between adjacent epochs of GLONASS R01, R02 and R03 for each analysis center on DOY 154, 155 in 2013. The clock correction differences in the same day were less than 0.3 ns; thus, the clock corrections are relatively continuous during the same day. However, the clock correction differences jump obviously at the day-boundary for NRCan, ESOC and GFZ analysis centers, and the jumps of the ESOC analysis center reach 12 ns. The clock drift of GLONASS R01, R02 and R03 is in only several picoseconds per second (Hauschild et al. 2013); thus, the changing of the clock corrections cannot reach up to 12 ns in a 30-s time span. The shown day-boundary jumps are caused by the changing of the clock references. Since the analysis centers select different reference stations on different days, GLONASS clock references vary; thus, day-boundary jumps occur in the GLONASS clock corrections.

In order to compute day-boundary jumps for each satellite, the clock corrections were extrapolated to the first epoch of the next day. First, the fitted clock drifts were calculated using the clock corrections of the last 10 min in the clock solution files. Then, the fitted clock corrections can be computed using fitted clock drift and the last epoch clock correction in the clock solution files,

$$\tilde{c}_a^s(t_2) = c_a^s(t_1) + v_c \Delta t \tag{9}$$

where $\tilde{c}_a^s(t_2)$ is the fitted clock correction of the first epoch of the next day, $c_a^s(t_1)$ is the clock correction of the last epoch provided by clock files, v_c is the fitted clock drift and Δt is the time interval. Since the fitted clock corrections are known, day-boundary jumps were obtained as:

$$\mathrm{DBJ}_a^s = c_a^s(t_2) - \tilde{c}_a^s(t_2) \tag{10}$$

where DBJ_a^s represents the clock day-boundary jumps and $c_a^s(t_2)$ represents the real first epoch clock correction provided by the clock solution files.

Figure 4 shows the day-boundary jumps for all the GPS and GLONASS satellites between DOY 154 and 155 in 2013 for each analysis center, the mean values and standard deviations (STDs). The maximum and minimum for each analysis center were computed and listed in Table 2. Thus, the GPS and GLONASS clock corrections exhibit both day-boundary jumps, but the day-boundary jumps in GPS are almost the same for each satellite. Furthermore, the GPS STDs of all the analysis centers are less than 0.3 ns. The differences between the maximum and the minimum values are all less than 1.3 ns. Unfortunately, the day-boundary jumps in GLONASS vary greatly. The GLONASS STDs of NRCan, ESOC, GFZ and IAC are significantly larger than that of GPS, reaching 0.619, 0.702, 0.506 and 0.365 ns, respectively. The differences between

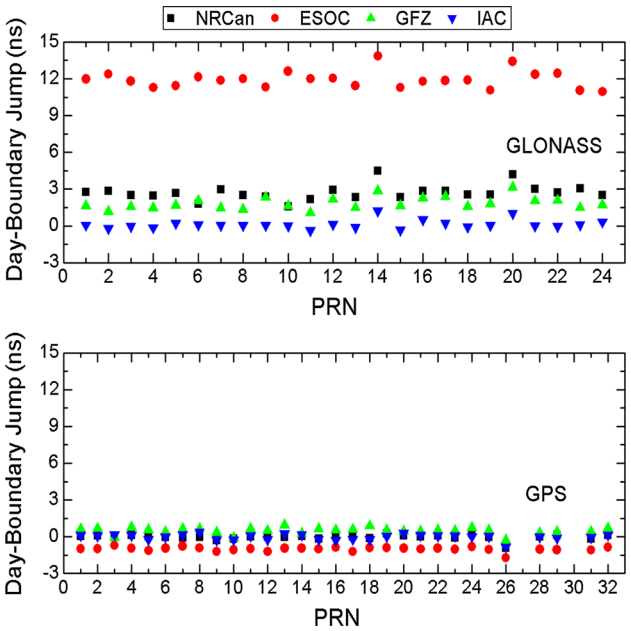

Fig. 4 The clock day-boundary jumps for all the GPS and GLONASS satellites for each analysis center between DOY 154 and 155 in 2013

the maximum and minimum values are also lager than that of GPS, reaching 2.9, 2.9, 2.1 and 1.6 ns, respectively. As the last epoch of clock corrections for ESOC, NRCan and IAC was 23:59:30 but that for GFZ was 23:55:00, when calculating the clock day-boundary jumps, GFZ needed 5 min extrapolation, while the other three analysis centers only needed 30-s extrapolation. However, the longer extrapolation time decreases day-boundary jump calculation accuracy.

Figure 5 shows the day-boundary jumps STDs of GPS and GLONASS for each analysis center from DOY 155 in 2012 to DOY 181 in 2013. Since a few of the GLONASS STDs are much larger than others, the *Y*-axis labeling of the middle panel is so large as to obscure the distribution of the GLONASS STDs. Therefore, the details are drawn in the bottom panel. Except for some individual STDs, the GPS STDs are less than 0.4 ns. The average STDs of NRCan, ESOC and IAC analysis center are 0.21, 0.23 and 0.22 ns, respectively. Since the extrapolation time is relatively longer for GFZ analysis center when calculating the day-boundary jumps, the average STD is slightly larger than that of the other three analysis centers, reaching 0.31 ns. For GLONASS, the day-boundary jumps STDs for each analysis center are much larger as compared to that of GPS because of the impact of pseudorange ICBs on the clock references. Some STDs can even reach up to dozens of nanoseconds. The average STDs for the NRCan, GFZ and IAC analysis centers reached 0.70, 0.49 and 0.31 ns, respectively, while the average STDs of the ESOC

Table 2 Mean values, standard deviations, maximum and minimum values for day-boundary jumps for each analysis center

ACs	NRCan (ns)		ESOC (ns)		GFZ (ns)		IAC (ns)	
	GPS	GLONASS	GPS	GLONASS	GPS	GLONASS	GPS	GLONASS
Average	−0.020	2.713	−1.002	11.926	0.502	1.842	−0.018	0.116
STDs	0.210	0.619	0.181	0.702	0.269	0.506	0.232	0.365
Maximum	0.257	4.506	−0.714	13.853	0.964	3.159	0.377	1.224
Minimum	−0.937	1.601	−1.714	10.941	−0.260	1.071	−0.831	−0.384

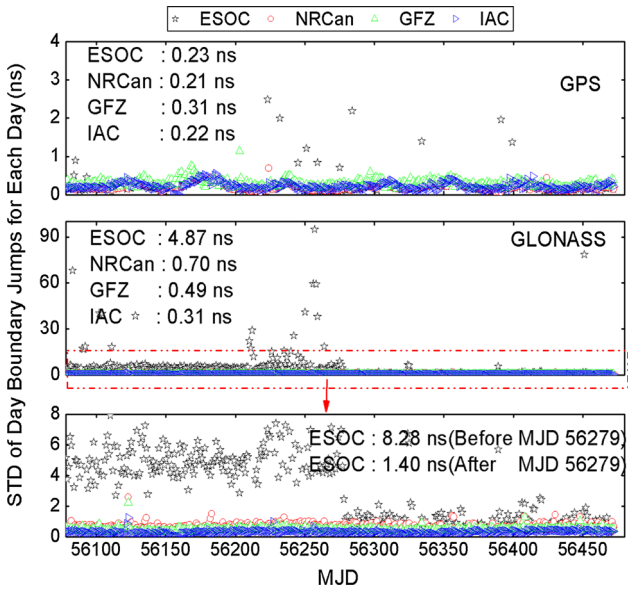

Fig. 5 Day-boundary jumps STDs of GPS and GLONASS for each analysis center from DOY 155 in 2012 to DOY 181 in 2013. The *top panel* shows the day-boundary jumps STDs of GPS for each analysis center, while the *middle* and the *bottom panel* show the STDs of GLONASS. The *bottom panel* is the partially enlarged detail of the GLONASS STDs since the *Y*-axis labeling of the *middle panel* is too large to show distribution of the GLONASS STDs clearly

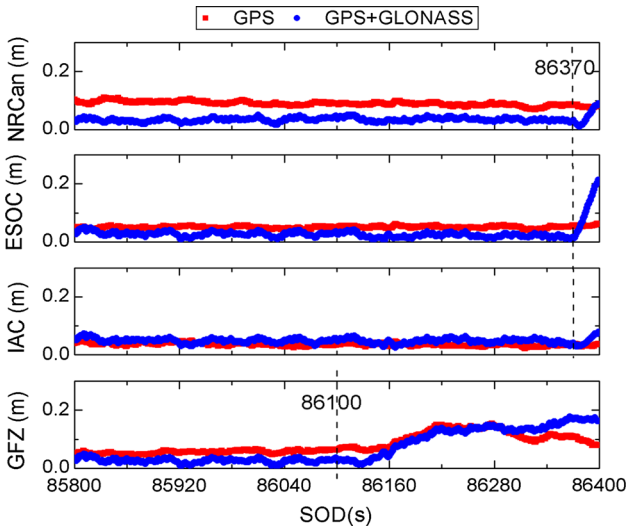

Fig. 6 3D deviations time series of GPS-only and combined GPS/GLONASS dynamic PPP solutions compared to the IGS weekly solutions at station ZIM2, at GPS time from 20:00:00 to 23:59:59 on DOY 154 in 2013. In order to show the variation more clearly, only the time series for the last 10 min is shown

Analysis Center reached up to 4.87 ns. The day-boundary jumps of the ESOC analysis center have significantly improved since MJD 56279 (18 Dec, 2012), the average STD was reduced from 8.28 to 1.40 ns.

Currently, each analysis center only provides GPS/GLONASS clock corrections with a 30-s interval (Table 1), but kinematic PPP applications require satellite clock corrections at a sampling rate equal to the observation rate, such as 1 HZ. The clock corrections between the intervals must be obtained by interpolation using the clock corrections before and after the observation epoch time (Hesselbarth and Wanninger 2008). But day-boundary jumps will lead to interpolation errors at the day-boundary. Moreover, only the shared portions of the interpolation errors for all satellites can be absorbed by receiver clock bias, while the remaining portions of the errors will affect PPP accuracy. Figure 6 shows the 3D deviations time series of GPS-only and combined GPS/GLONASS dynamic PPP solutions compared to the IGS weekly solutions at station ZIM2, at GPS time from 20:00:00 to 23:59:59 on DOY 154 in 2013. The data sample was 1 Hz and the weight ratio of GLONASS and GPS observations in the least-squares adjustment was set to 1:2. The accuracies of the combined GPS/GLONASS PPP were superior to that of GPS-only PPP as illustrated in Fig. 6. For the NRCan analysis center, there were about 10 cm systematic errors after PPP convergence, while the systematic errors in the combined GPS/GLONASS PPP were significantly reduced. But the accuracies of the combined GPS/GLONASS PPP decreased significantly from the second of day (SOD) 86,370, while this phenomenon did not appear in the GPS-only PPP. This is because the differences in the GPS day-boundary jumps for each satellite were small. As a consequence, most of the interpolation errors in satellite clock corrections were absorbed into the receiver clock bias and have little effect on PPP. But for GLONASS, the day-boundary jumps vary shapely for each satellite so that the interpolation errors cannot be absorbed by the receiver clock bias and will

affect the combined GPS/GLONASS PPP at the day-boundary. Since the last epoch of GFZ clock corrections was 23:55:00 (SOD 86100 s), the time interval of clock interpolation was too long, and therefore, the clock interpolation accuracy reduced, so the combined GPS/GLONASS PPP accuracy began to decline from SOD 86100. The GPS-only PPP accuracy was also reduced.

Furthermore, as can be seen in Table 2, the day-boundary jump STD for ESOC clock corrections was maximal and had the greatest impact on the PPP accuracy. The day-boundary jump STD for the IAC clock corrections was minimal and had the minimal impact on the PPP accuracy, indicating that the impact magnitude of day-boundary jumps on combined GPS/GLONASS PPP is related to the day-boundary jump STDs.

GNSS clock solution combination

The combined GPS/GLONASS PPP can improve the accuracy, reliability and the acceleration of PPP convergence (Cai and Gao 2007, Hesselbarth and Wanninger 2008). However, the GLONASS clock day-boundary jumps differ greatly between satellites for each analysis center, affecting the accuracy of the combined GPS/GLONASS PPP at the day-boundary. Currently, the IGS only provides GPS precision clock solutions but no GLONASS precise clock solutions, so it is necessary to provide the combined GPS/GLONASS precision clock solutions. The GLONASS orbit combination can use the same method as that of GPS and the orbits accuracies of NRCan, ESOC, GFZ and IAC are close to each other, up to centimeter (http://acc.igs.org). As a consequence, orbit combination is not discussed here.

Before combining clock corrections, the clock references for each satellite must be eliminated (Kouba and Springer 2001). Since the AC-specific offsets and the satellite and AC-specific offsets of the GLONASS clock corrections both differ sharply between analysis centers, they are estimated during clock combination. From (6), it can be obtained:

$$c^s_{i,sys} = c^s_{sys} + o_{i,sys} + o^s_{i,sys} \tag{11}$$

where sys represents the GPS or GLONASS system, $c^s_{i,sys}$ represents the clock corrections of analysis center i, $o_{i,sys}$ and $o^s_{i,sys}$ represent the AC-specific offsets and satellite and AC-specific offsets of analysis center i and c^s_{sys} represents the combined clock corrections.

When estimating the parameters, c^s_{sys} is considered as a random walk process, $o_{i,sys}$ is white noise and $o^s_{i,sys}$ is a constant within 24 h. Equation (11) shows that c^s_{sys}, $o_{i,sys}$ and $o^s_{i,sys}$ are linear dependent, so the $o^s_{i,sys}$ for each analysis center and c^s_{sys} were constrained as:

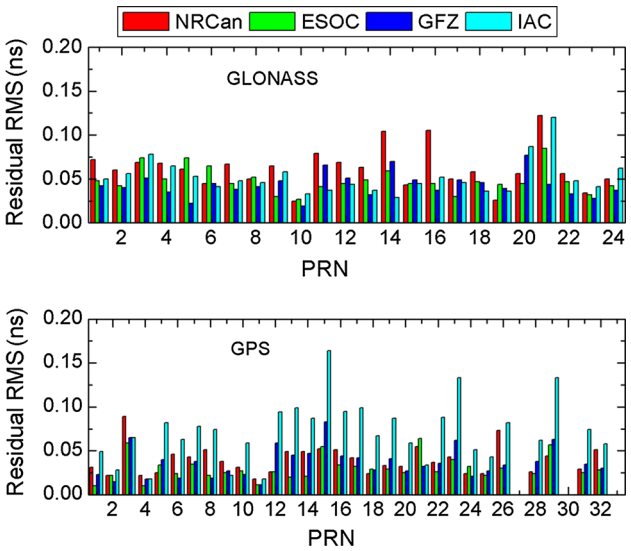

Fig. 7 RMS of the combination residuals for each satellite on DOY 154 in 2013

$$\sum_{s=1}^{m} o^s_{i,sys} = 0 \qquad \sum_{s=1}^{m} c^s_{sys} = 0 \tag{12}$$

where m represents the number of satellite GPS or GLONASS system. In order to improve the accuracy of the combined clock corrections at the initialization time, an inverse filter was used.

Figure 7 shows the RMS of the combination residuals for each satellite on DOY 154 in 2013. The clock corrections of each analysis center are considered to be equal weight during the clock combination. All the RMS of the combination residuals in Fig. 7 are less than 0.15 ns, while most of them are less than 0.05 ns. So the clock combination algorithm presented here is feasible. However, the RMS of GPS combination residuals for IAC in this figure are significantly larger than that of other analysis centers, indicating that the IAC GPS clock correction accuracy is the least satisfactory among the analysis centers on DOY 154 in 2013.

Figure 8 displays the daily estimations of GLONASS satellite and AC-specific offsets for each analysis center on DOY 154–157 in 2013. To illustrate the stability of these estimations in different days, the STDs of the estimations were computed and shown in Fig. 9. As these figures reveal, the GLONASS satellite and AC-specific offsets of each analysis center are relatively stable. The average STDs of GFZ and IAC are only 0.15 ns. The GPS satellite and AC-specific offsets of each analysis center are smaller than that of GLONASS, mostly less than 0.1 ns. Therefore, the estimations are not presented here.

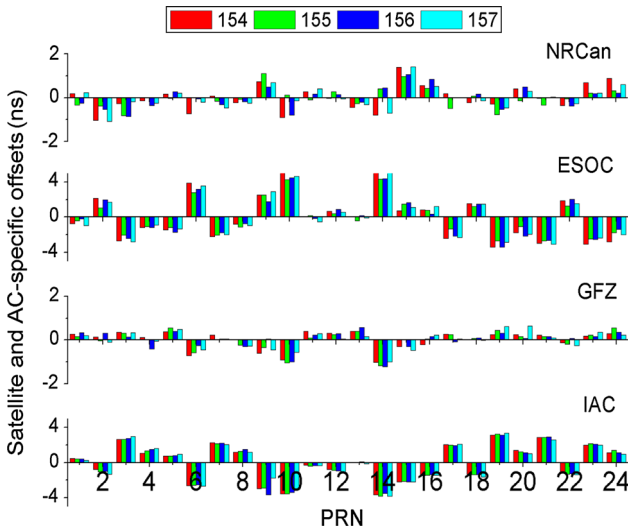

Fig. 8 Satellite and AC-specific offsets valuations of each analysis center on DOY 154–157 in 2013

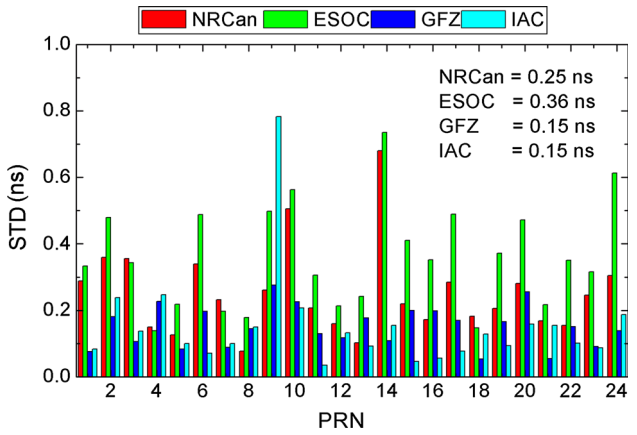

Fig. 9 STD of the satellites and AC-specific offset valuations in different days of each analysis center and the average STDs are shown on the *upper right corner*

As the combined clock corrections obtained by (11) and (12) lack clock references, they must be provided. The GLONASS satellite and AC-specific offsets of GFZ and IAC are the most stabile between days. But the IAC GPS clock correction accuracy is the least satisfactory among the analysis centers, so the GFZ clock references were selected as the combination clock references. To further reduce the impact of the day-boundary jumps, the weighted average of the satellite and AC-specific offsets over the adjacent two days was used as the satellite and AC-specific offsets for the second day.

In order to test whether the combination clock corrections can weaken the effects of the day-boundary jumps on the combined GPS/GLONASS PPP, the data in Fig. 6 were reprocessed using the combination clock corrections. Figure 10 presents the reprocessed time series solutions; the

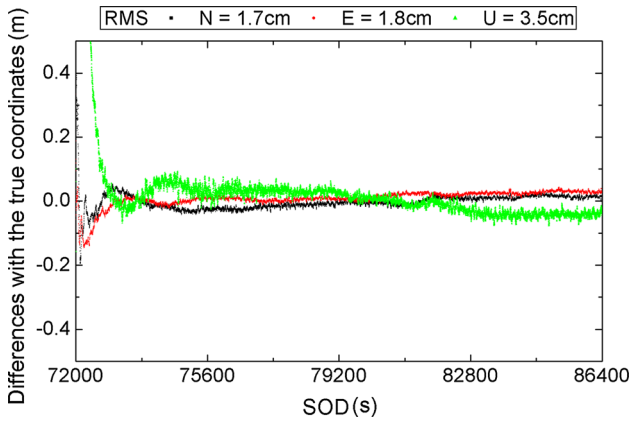

Fig. 10 Time series of the reprocessed solutions with the data in Fig. 6

combined GPS/GLONASS PPP accuracy did not become significantly worse at the day-boundary when using the combination clock corrections. This indicates that the impact of day-boundary jumps can be significantly weakened. The RMS of N, E, and U components reach 1.7, 1.8 and 3.5 cm, respectively, using the combination clock corrections.

Figure 11 shows the RMS statistics of the combined GPS/GLONASS static PPP single-day solutions using different clock corrections of 120 IGS stations on DOY 154 in 2013. The best results are from the GFZ, with a RMS of 0.4, 0.6 and 1.3 cm in the East, North and Up components, respectively. The IAC results are the least satisfactory, with the RMS for East, North and Up components at 1.5, 1.0 and 2.0 cm, respectively. This is because the IAC GPS clock correction accuracy is the least satisfactory among the analysis centers. Fortunately, the accuracy is further improved after clock combination, with RMS in the East, North and Up components at 0.3, 0.6 and 1.3 cm, correspondingly. As compared to IAC, the accuracy of the combined GPS/GLONASS PPP using combined clock corrections is improved by 80, 40 and 35 % in the East, North and Up components, in that order.

Conclusions

We analyzed the effect of GLONASS pseudorange interchannel biases on the GLONASS clock corrections reference. There were three significant findings. First, different analysis centers eliminate the impact of GLONASS pseudorange ICBs in different ways which leads to significant differences in satellite and AC-specific offsets for GLONASS clock corrections. Second, the satellite and AC-specific offset differences are strongly correlated with frequency number. Third, the GLONASS pseudorange ICBs also lead to day-boundary jumps in GLONASS

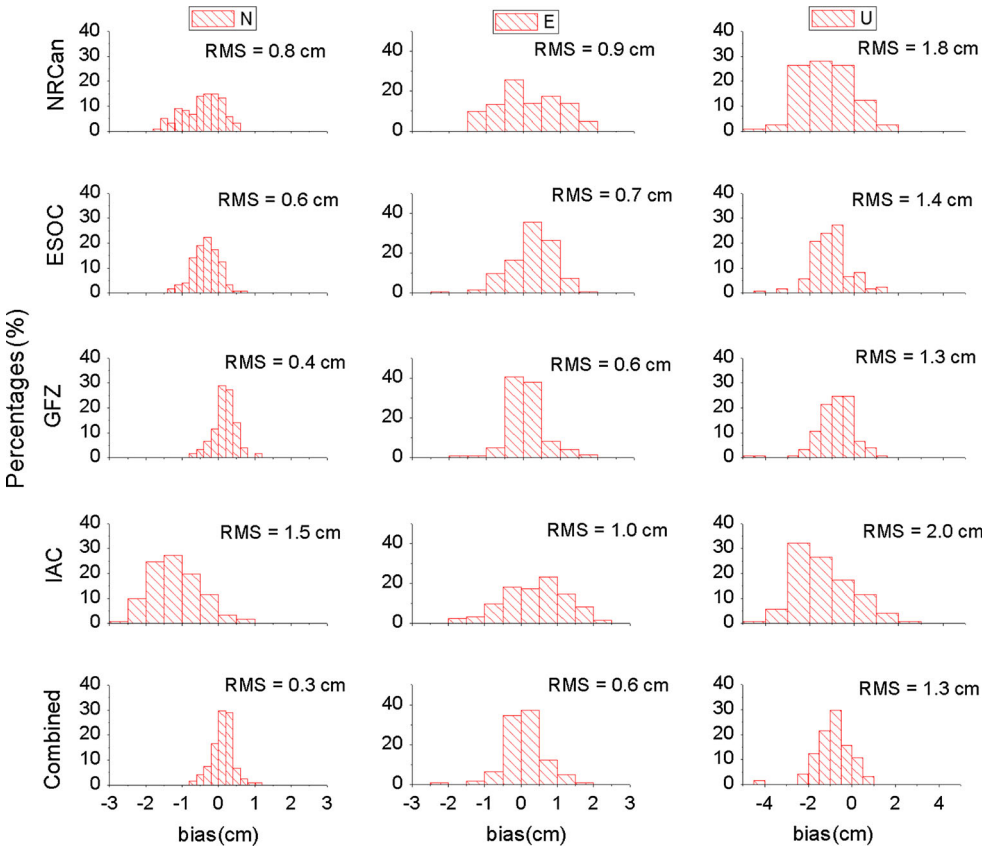

Fig. 11 RMS statistics for the combined GPS/GLONASS static PPP single-day solutions of 120 IGS stations on DOY 154 in 2013. The panels from the *top* to the *bottom* represent the clock corrections results of NRCan, ESOC, GFZ, IAC and combined clock results, respectively. The weight ratio of GLONASS and GPS observations in the least-squares adjustment is set as 1:2, and the real coordinates were provided by the IGS weekly solutions

clock corrections for the same analysis center between adjacent days. This in turn will influence the accuracy of the combined GPS/GLONASS PPP at the day-boundary. Given these three factors, it is recommended that analysis centers use the same preprocessing strategy for GLONASS pseudorange ICBs and provide these corrections to users.

Additionally, we propose a GNSS clock correction combination method and give some preliminary test results. These results show that combined clock corrections can effectively weaken the influence of clock day-boundary jumps on the combined GPS/GLONASS dynamic PPP. Furthermore, the combined clock corrections can improve the accuracy of the combined GPS/GLONASS static PPP single-day solutions as compared to accuracy of each analysis center alone. This illustrates the feasibility and effectiveness of the proposed clock combination method. However, there are still some improvements to be made in the clock combination method. First, the proposed combination clock references simply select the clock references of GFZ and should be unified to the IGS time scales. Second, the impact of the GLONASS pseudorange ICBs on the clock reference must be eliminated. Third, we did not detect the clock correction outliers and those must be detected. Fourth, we assumed equal weight for each analysis center, but it is preferable to set the weight ratios according the clock corrections accuracy for each analysis center.

Acknowledgments We thank Simon Banville, at NRCan, and Maorong Ge, at GFZ, for their valuable suggestions on this study. The IGS is acknowledged for providing high-quality combined GPS/GLONASS precise orbit and clock corrections as well as tracking data. This study was supported by the National Natural Science Funds (Grant No. 41374034), the National High Technology Research and Development Program of China (863 Program) (Grant No. 2012AA12A202) and also by China Postdoctoral Science Foundation (Grant No. 2012M511671).

References

Bisnath S, Gao Y (2008) Current state of precise point positioning and future prospects and limitations. In: Sideris MG (ed) Observing our changing Earth. Springer, New York, pp 615–623

Bock H, Dach R, Jäggi A, Beutler G (2009) High-rate GPS clock corrections from CODE: support of 1 Hz applications. J Geodesy 83:1083–1094

Cai C, Gao Y (2007) Performance analysis of precise point positioning based on combined GPS and GLONASS. In: Proceedings of ION GNSS-2007, Institution of Navigation, Fort Worth, Texas, September, pp 858–865

Chuang S, Wenting Y, Weiwei S, Yidong L, Yibin Y, Rui Z (2013) GLONASS pseudorange inter-channel biases and their effects on combined GPS/GLONASS precise point positioning. GPS Solutions, GPS Solutions 17(4):439–451

Ge M, Chen J, Douša J, Gendt G, Wickert J (2012) A computationally efficient approach for estimating high-rate satellite clock corrections in realtime. GPS Solutions 16(1):9–17

Hauschild A, Montenbruck O, Steigenberger P (2013) Short-term analysis of GNSS clocks. GPS Solutions 17(3):295–307

Hesselbarth A, Wanninger L (2008) Short-term stability of GNSS satellite clocks and its effects on precise point positioning. In: Proceedings of ION GNSS-2008, Institution of Navigation, San Diego, California, September, pp 1855–1863

Kouba J (2003) A guide to using International GPS Service (IGS) products. IGS report, International GPS Service

Kouba J, Héroux P (2001) Precise point positioning using IGS orbit and clock products. GPS Solut 5(2):12–28

Kouba J, Springer T (2001) New IGS station and satellite clock combination. GPS Solut 4(4):31–36

Kozlov D, Tkachenko M, Tochilin A (2000) Statistical characterization of hardware biases in GPS + GLONASS receivers. In: Proceedings of ION GPS-2000, U.S. Institution of Navigation, Salt Lake City, Utah, September, pp 817–826

Mervart L, Weber G (2011) Real-time combination of GNSS orbit and clock correction streams using a Kalman filter approach. In: Proceedings of ION GNSS-2011, Institution of Navigation, Portland OR, September, pp 707–711

Píriz R, Calle D, Mozo A, Navarro P, Rodríguez D, Tobías G (2009). Orbits and clocks for GLONASS precise-point-positioning. In: Proceedings of ION GNSS-2009, Institution of Navigation, Savannah, Georgia, September, pp 2415–2424

Reussner N, Wanninger L (2011) GLONASS inter-frequency biases and their effects on RTK and PPP carrier-phase ambiguity resolution. In: Proceedings of ION GNSS-2011, Institution of Navigation, Portland OR, September, pp 712–716

Wanninger L (2012) Carrier phase inter-frequency biases of GLONASS receivers. J Geodesy 86(2):139–148

Zhang X, Li X, Guo F, Li P, Wang L (2010) Server-based real-time precise point positioning and its application. Chin J Geophys Chin Edit 53(6):1308–1314

Zumberge JF, Heflin MB, Jefferson DC, Watkins MM, Webb FH (1997) Precise point positioning for the efficient and robust analysis of GPS data from large networks. J Geophys Res 102(B3):5005–5017

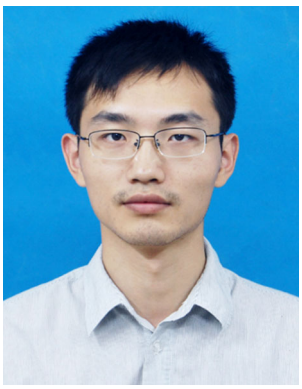

Weiwei Song is currently a post-doctorate fellow at the Wuhan University. He has obtained his PhD degree from Wuhan University, P.R.C., in 2011. His current research mainly focuses on real-time GNSS precise positioning technology.

Wenting Yi is currently a PhD student at the Wuhan University. He has obtained his Bachelor's degree from Wuhan University, P.R.C., in 2009. His current research focuses mainly involve GNSS precise positioning technology.

Yidong Lou is currently an Associate Professor at GNSS Research Center, Wuhan University. He obtained his PhD in Geodesy and Surveying Engineering from the Wuhan University in 2008. His current research interest is in the real-time precise GNSS Orbit determination and real-time GNSS precise point positioning. He is one of the members who have developed the PANDA software which has been widely used in china.

Chuang Shi is the head for GNSS Research Center of Wuhan University. He graduated from Wuhan University and obtained his PhD degree in 1998. His research interests include network adjustment, precise orbit determination of GNSS satellites and LEOs and real-time precise point positioning (PPP).

Yibin Yao is currently a professor at the Wuhan University. He obtained his B.Sc., Master and Ph.D. degrees with distinction in Geodesy and Surveying Engineering at the School of Geodesy and Geomatics in Wuhan University in 1997, 2000 and 2004. His main research interests include GPS/MET and high-precision GPS data processing.

Yanyan Liu is currently a PhD student at the Wuhan University. He has obtained his Bachelor's degree from Wuhan University, P.R.C., in 2009. His current research focuses mainly involve GNSS precise positioning technology.

Yong Mao is a manager in PetroChina West East Gas Pipeline Company. He has obtained his Bachelor's degree from Southwest Jiaotong University, P.R.C., in 2008. His current research focuses mainly involve the practical application of GNSS.

Yu Xiang is currently working at Wuhan University. He has served as a senior software engineer for 6 years in Geomatics Information Center of Hubei Province. His research focuses mainly on the practical application of GNSS and GIS.